J. Indian Inst. Sci., May–Aug. 2002, **82**, 145–160

Thermochromic liquid crystals for assessing the performance of scramjet inlets with notched cowls

DAVID J. MEE*, MICHAEL D. SKOWRONSKI AND H.-H. SAM CHIU
Department of Mechanical Engineering, The University of Queensland, Brisbane QLD 4072, Australia.
Email: mee@mech.uq.edu.au; Phone: +61-7-3365-4058.

Received on May 21, 2002

Abstract

Broadband thermochromic liquid crystals have been used to investigate the heat-transfer properties of geometries characteristic of scramjet inlets in a Mach 3 flow. The models tested comprised opposing 17° wedges that generate colliding shocks that can interact with boundary layers formed on an end wall. In one case, the end wall had a straight leading edge and in the other the leading edge was notched. The results indicate that heat-transfer rates and inlet separation can be reduced by using a notched cowl.

Keywords: Liquid crystals, heat-transfer measurement, scramjet, shock wave boundary layer interaction.

1. Introduction

Aerospace vehicles travelling at super and hypersonic speeds are exposed to high heating rates. Heat-transfer rates to model vehicles can be measured in ground-based testing facilities using a variety of techniques. Most techniques are based on discrete sensors placed on the surface of a test model (e.g. thin-film, calorimeter and thermocouple gauges). More detailed information about the spatial variations in heating rates can be obtained using surface coatings such as thermal paints or thermographic phosphors that can potentially indicate the heat-transfer rates to the entire model. Another type of surface coating, thermochromic liquid crystals (TLCs), can also be used to measure the surface temperatures on wind tunnel models. TLCs change colour with temperature and in microencapsulated form are, for the most part, insensitive to effects of pressure and surface shear. Some advantages of TLC coatings over techniques involving other surface coatings are that illumination only in the visible spectrum is required, images can be recorded on video tape without the need for special optics or filters and the colour changes in the liquid crystal layer are reversible and repeatable.

Liquid crystal coatings were first applied to aerothermal testing by Klein [1]. Since then, their use in heat-transfer measurement in low-speed flows has been extensive [2]–[4]. While TLCs have not been used much in supersonic flows, they have been applied for heat-transfer indication in transonic flows [5] and even in hypersonic flows [6], [7].

For heat transfer to take place there must be a driving temperature difference between the test gas and the model. One of the reasons liquid crystals have been used more in hypersonic than in supersonic flows is that the test gas is heated in most hypersonic test facilities. With test models starting at room temperature, there is then a driving temperature difference for heat transfer to

*Author for correspondence.

occur. A very simple and common type of supersonic flow test facility is the blowdown wind tunnel. In this type of tunnel, air is discharged from a high-pressure reservoir through a converging–diverging nozzle and through the test section of the tunnel. It is usually only necessary to heat the air, either in the reservoir or prior to it flowing through the test section, if test Mach numbers in excess of about four are required. (For higher Mach numbers, liquefaction of the air may otherwise occur at the low temperatures generated in the test section.) Heat-transfer measurement in unheated blowdown tunnels has usually not been attempted because of the complexity involved in heating or cooling the test model prior to a test but this has been done [5], [8].

There does exist a natural temperature difference between the model and the test gas in an unheated supersonic blowdown wind tunnel, albeit a small one. If both the model in the test section and the test gas in the reservoir start at ambient temperature, then the recovery temperature (or adiabatic wall temperature) of the flow in boundary layers on the test model will typically be lower than the stagnation temperature of the test gas. The higher the Mach number, the higher the temperature difference will be. The surfaces of the test model will then cool during a test and the rate at which the surfaces cool can be used to infer the heat-transfer rate. This has been used in some tests to measure heat-transfer rates using discrete sensors [9] and it has recently been shown that narrowband TLCs can be used for heat-transfer indication with such driving temperatures in a supersonic blowdown tunnel [10].

The purpose of the present paper is to demonstrate the use of broadband TLCs in a Mach 3 blowdown tunnel to infer the relative heat-transfer rates of different inlet configurations for supersonic combustion ramjets (scramjets). The significance of the inlet geometries tested is presented in Section 2 and some features of a notched inlet are introduced in Section 3. The details of the experimental equipment and procedures are described in Section 4 and the results are presented in Section 5.

2. Scramjet inlets

Inlets for air-breathing engines for high-speed flight, such as scramjets, must reduce the speed of the gas entering the engines as efficiently as possible. Two of the main problems associated with such inlets are those of maintaining a started inlet (i.e. ensuring that the inlet always supplies a supersonic flow into the burner) and maintaining the structural integrity of the inlet in the harsh thermal environment.

There are two simple types of inlet compression that are most often considered for scramjets. The first is a two-dimensional compression inlet (Fig.1) in which the forebody of the vehicle produces some compression and the cowl of the engine produces further compression [11], [12]. The other common type of inlet produces three-dimensional flow and uses the sidewalls of the inlet to provide (additional) compression (Fig. 2). This is the so-called sidewall compression inlet [13], [14]. For both types of inlets, engine unstart may occur if the interactions of the shock waves with boundary layers formed on the surfaces of the inlet lead to boundary layer separation. One potential advantage of the sidewall compression inlet is that the intersecting shock compression may be able to produce a larger overall pressure rise without separating the boundary layer than can a 2D compression inlet [15]. A simplified model of the sidewall compression inlet is the subject of the present paper.

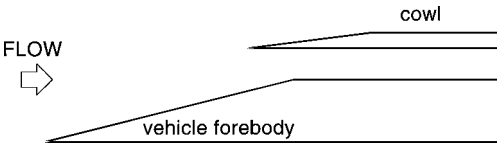

FIG. 1. Two-dimensional, two-shock, scramjet inlet.

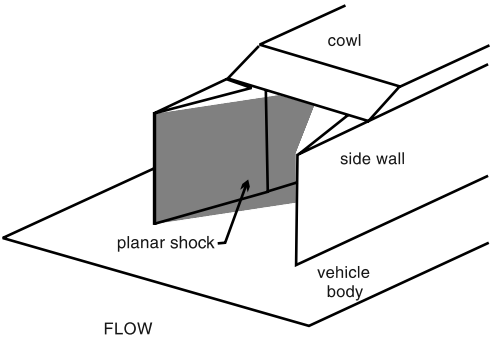

FIG. 2. Generic sidewall compression scramjet inlet.

The basic idea of the sidewall compression inlet shown in Fig. 2 is to achieve the inlet compression through shocks generated by the inner surfaces of the two sidewalls that are inclined to the oncoming flow. The resulting shock waves, that are planar in the simplified arrangement shown in Fig. 2, intersect and reflect. The shocks interact with the boundary layers formed on the endwalls (in this case the vehicle body and the cowl). This is sometimes referred to as a colliding shock wave boundary layer interaction and was first studied by Mee *et al.* [15]. There has been much subsequent study of this type of geometry both from a fundamental point of view [8], [16] and for scramjet inlet applications [17]. In some applications for scramjet inlets the leading edges of the sidewalls are also swept back, to assist in inlet starting at lower Mach numbers [18].

Note that the cowl in Fig. 2 is located aft of the leading edges of the sidewalls that compress the oncoming flow. This is also done to assist in starting the inlet at low Mach numbers. Korte *et al.* [19] suggest that judicious aft cowl placement can assist in inlet starting at the lower Mach numbers by spilling some of the flow that would otherwise enter the engine but that "unfortunately the low-speed starting problem typically hinders the high-speed performance characteristics''. One problem with this type of arrangement is that there will be flow spillage even at the design Mach number.

An alternative to simply moving the cowl aft is to start the cowl at the leading edges of the sidewalls but to sweep the cowl's leading edges, thus creating a notch in the cowl (see Fig. 3). This type of notched-cowl and similar arrangements have been proposed for a number of scramjet inlets [20]–[22]. The notched arrangement has the same beneficial properties for flow starting at low Mach numbers as the aft-cowl arrangement of Fig. 2. For the simple arrangement shown in Fig. 3, the sweep angle of the leading edges of the cowl can be set to be close to the sweep angle of the shock waves generated by the sidewalls at the design Mach number. If that is done, there will be no spillage of flow at the design condition. At lower Mach numbers, the shock waves generated by the sidewalls will be more oblique and there will be flow spillage to assist in starting the inlet.

There are other potential advantages of sweeping the leading edges of the cowl along the line of sweep of the sidewall shock waves that have not been addressed in the literature. These are discussed in Section 3.

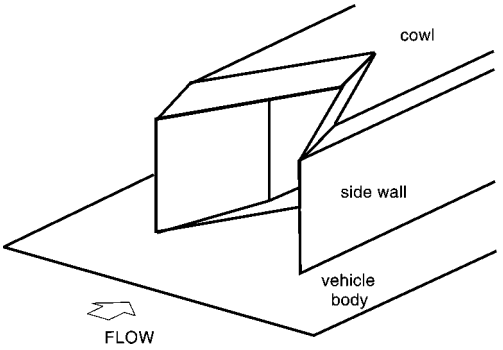

FIG. 3. Sidewall compression scramjet inlet with notched cowl.

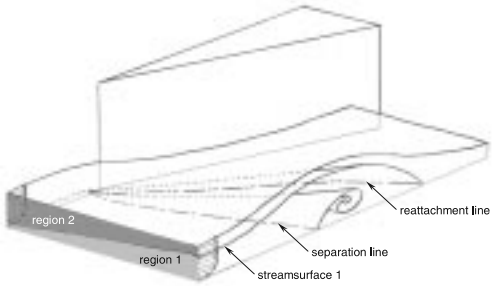

FIG. 4. Flow structure for a separated interaction generated by a single wedge (adapted from Knight *et al*. [24].

3. Other potential advantages of a notched inlet

In addition to the good starting capabilities at low Mach number and no spillage at the design Mach number, there are two other potential advantages of the notched inlet that can be explained with reference to the flow field generated by a single wedge interaction. When a shock wave generated by a wedge normal to a plate interacts with a boundary layer formed on that plate, the slow-moving flow in the boundary layer is deflected more by the spanwise pressure gradient than is the faster-moving flow outside the boundary layer. This leads to a severe twisting of the boundary layer. At a certain shock strength a form of 3D boundary layer separation occurs [23]. A sketch of the flow field for a separated interaction, adapted from Knight *et al.* [24], is shown in Fig. 4. The oncoming flow is divided by a streamsurface into two regions. The flow between the endwall and streamsurface 1, region 1, is entrained into the vortical structure. The flow above that surface, region 2, passes over the vortical structure and reattaches downstream. A conical development of such interactions, as proposed by Settles and Lu [25], means that, away from the wedge, it is possible that flow from outside the boundary layer can be entrained into the separation vortex.

Such a flow structure leads to regions of reduced heat transfer near the line of separation and increased heat transfer near lines of reattachment. The entrainment of flow into the vortex also leads to an effective increase in the displacement thickness of the boundary layer in the vicinity of the vortical structure. Some increase in heat transfer would be expected due to the higher densities and pressures behind the shock but measurements indicate that peak heat-transfer rates near the reattachment line can be of the order of four to five times the undisturbed flat plate values and twice as high as can be attributed to the increased pressure [26].

If the boundary layer is started at or just downstream of the shock wave, as can be achieved if the leading edge of the notched inlet follows the line of the shock from the wedge, then the boundary layer on the endwall will form in a region of uniform pressure. Thus the boundary-layer twisting phenomenon and the shock-induced separation will be avoided. An increase in heat transfer over that without a wedge would be expected, but the very high values near reattachment may not be attained. Secondly, the increased displacement thickness of the boundary layer associated with boundary layer separation should be avoided.

If such a notched inlet does avoid the boundary layer separation, then, in addition to advantages for starting the inlet at low Mach numbers, the notched inlet may also lead to (1) reduced heat transfer to the cowl, and (2) less reduction in the cross section the inlet presents to the inflow due to reduced displacement thickness. The present series of experiments was designed to see if the notched inlet achieves these effects.

4. Experimental

The experiments were performed in The University of Queensland (UQ) Supersonic Blowdown Tunnel. This is a small facility with a 115 x 100 mm test section. A Mach 3 nozzle was installed for the present tests. Typical conditions for the tests were 625 kPa stagnation pressure and 295 K starting stagnation temperature, giving a unit Reynolds number in the test section of 4.8×10^7 m^{-1}. The total pressure and total temperature of the flow were measured in a plenum chamber ahead of the nozzle. The flow Mach number is based on the measured total pressure and a measurement of the static pressure taken on the side wall of the tunnel just ahead of the model.

One feature of the facility used for the present tests is that the stagnation temperature decreases during a test. The test gas is supplied from a large reservoir and, as the gas is discharged through the tunnel the pressure in the reservoir decreases. This is accompanied by a decrease in the temperature of the gas and thus a decrease in stagnation temperature of the test flow during a test. For heat transfer to models in the test section when the recovery factor is less than unity, this means a continual decrease in model temperature during a test.

The four basic geometries shown in Fig. 5 were tested. They consist of wedges mounted normal to the endwall to simulate the sidewalls of a scramjet inlet. The endwall, to which the wedges are attached, simulates the cowl of an inlet. Two endwall configurations were tested, one with a straight leading edge and the other with a notch. Of relevance for the scramjet inlet are the double-wedge configurations but the single-wedge configurations are useful for identifying the flow features. Since only the inlet portion of the scramjet was of interest here, the flow was expanded again immediately after the compression. It should be noted that this decouples any effect that the flow in a combustor would have on inlet performance.

The test models were made of perspex. The chord of the wedges was 39 mm and their span 20 mm. The included angle of the leading edge of the wedges was 17° and the rear of the wedge had an included angle of 27°. For such small size models, laminar boundary layers are expected with the Reynolds number based on the length of the 17° portion of the wedge (25 mm) and the freestream conditions being approximately 1.2×10^6. For single wedge interactions, results from Degrez and Ginoux [27] indicate similar flow features for laminar interactions to those observed

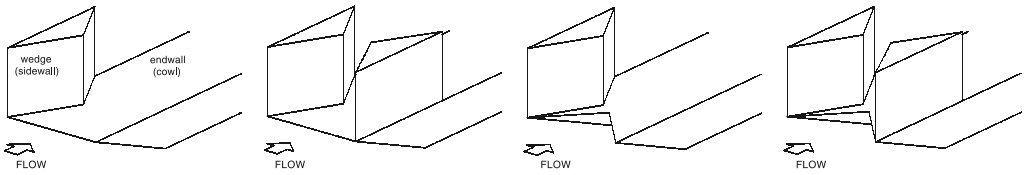

FIG. 5. The four model geometries tested. (a) Straight leading edge, single wedge. (b) Notched leading edge, single wedge. (c) Straight leading edge, double wedge. (d) Notched leading edge, double wedge.

Table I
Nominal colour play temperatures for R0C20W liquid crystal

Colour	Temperature (°C)
Visible start	−0.8
Red start	0.0
Green start	4.3
Bright green	9.5
Blue start	22.8
Colourless	29.3

in the turbulent interactions that have been studied more extensively. However, boundary layer separation occurs for weaker interactions in laminar flows [27].

At Mach 3, the oblique shocks generated by the wedges on the models will be at an angle of 34.4° to the flow. The notch in the notched inlet was swept back at that angle. The leading edges of the endwalls had 30° included angles and the endwalls were 25 mm wide and 15 mm thick. A static pressure tapping was located on the wedge, 11.5 mm from the leading edge and 8.5 mm above the surface of the endwall.

The endwalls were sprayed with a thin layer of matt black paint. Broadband thermochromic liquid crystals were sprayed on top of the paint layer. The total thickness of such layers is about 20 μm (see Ireland and Jones [3]). The liquid crystal used was supplied by Hallcrest U.K. Ltd and was designated R0C20W. The liquid crystal layer was not calibrated after being sprayed onto the test surface for the present tests since only qualitative information about heat-transfer rates was sought. The nominal colour play ranges for the mixture used are listed in Table I.

The models were mounted from the sidewalls of the tunnel. The roof of the test section had a 50 mm thick perspex window in it. A video camera was located directly above the test section and fluorescent lighting was used to illuminate the model through the window so that the colour play could be recorded. The arrangement is similar to that described in more detail in Mee *et al.* [10]. The major difference between the techniques used here and those reported in reference [10] is that a broadband liquid crystal was used in the present experiments while a mixture of two, narrowband (approximately 1° C) crystals was used in the other study. Results from those experiments were processed to infer quantitative measurements of heat transfer but the broadband liquid crystals employed here were used only to obtain a visualization of the relative heat-transfer levels over the endwall. It is shown in Section 5 that flow features can also be inferred from the broadband liquid crystal visualization.

5. Results

5.1. *Single wedge cases*

Test number 42 had the endwall with a straight leading edge and a single wedge (the configuration in Fig. 5a). The pressures measured during the test are shown in Fig. 6. The stagnation pressure rises rapidly and remains approximately constant (within ±2%) during the test period of approximately 12 s duration. The zero for the time scale in the plot is taken as the time when stagnation temperature reaches a peak (see below). Shown also in Fig. 6 are the freestream static

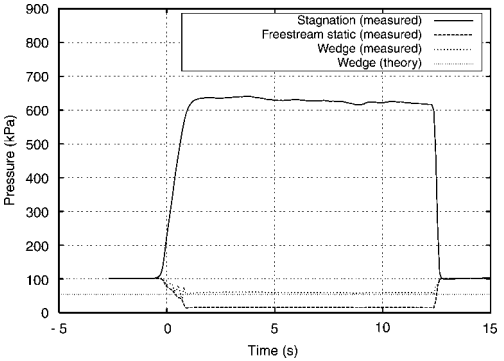

FIG. 6. Pressures for test 42 (straight leading edge, single wedge).

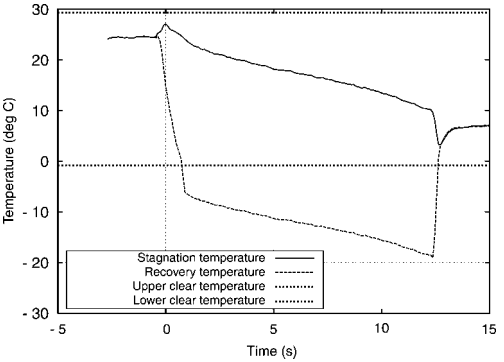

FIG. 7. Temperatures for test 42 (straight leading edge, single wedge).

pressure, measured at a sidewall pressure tapping just upstream of the model, and the pressure measured on the wedge. The latter is close to the value predicted from oblique shock theory.

The ambient temperature before test 42 was approximately 24° C. The stagnation temperature measured during the test is shown in Fig. 7. When the test commences, the gas in the plenum chamber ahead of the nozzle is rapidly compressed and its temperature rises. This is why there is a small increase in temperature at the start of the trace. The gas in the plenum is quickly vented through the test section and the temperature drops again. Then as the pressure of the gas in the supply reservoir decreases, the stagnation temperature decreases steadily during the test. When comparing results from different tests, the reference time will be taken as the time of peak stagnation temperature; thus the peak occurs at time zero in Fig. 7.

Shown also in Fig. 7 is an indication of the recovery temperature on the model surface during the test. The recovery temperature, T_r, can be related to the stagnation temperature, T_0, for a given Mach number, M, and ratio of specific heats, γ, in terms of a recovery factor, r,

$$T_r = T_0 \frac{1 + r\frac{\gamma-1}{2}M^2}{1 + \frac{\gamma-1}{2}M^2}. \tag{1}$$

The value to use for the recovery factor in regions of shock/boundary-layer interactions is uncertain [26] but for a laminar boundary layer in the absence of pressure gradients, a typical value is 0.845. This value has been used with eqn (1) to produce the trace shown in Fig. 7. The recovery temperature was calculated at each point in time using the Mach number determined from the measured stagnation and static pressures. It should be noted that the recovery temperature trace in Fig. 7 is only an estimate of the recovery temperature for the plate. The recovery factor would be expected to vary in different regions of the interaction [26]. However, the estimate is useful for identifying the levels of temperatures expected.

Figure 7 also shows the nominal lower and upper clearing temperatures for the liquid crystal (see Table I). It can be seen that the stagnation temperature, which is also approximately the temperature at which the model starts, is within the colour play range of the liquid crystal. Once the supersonic flow is established, the temperature to which the plate is being driven (the recov-

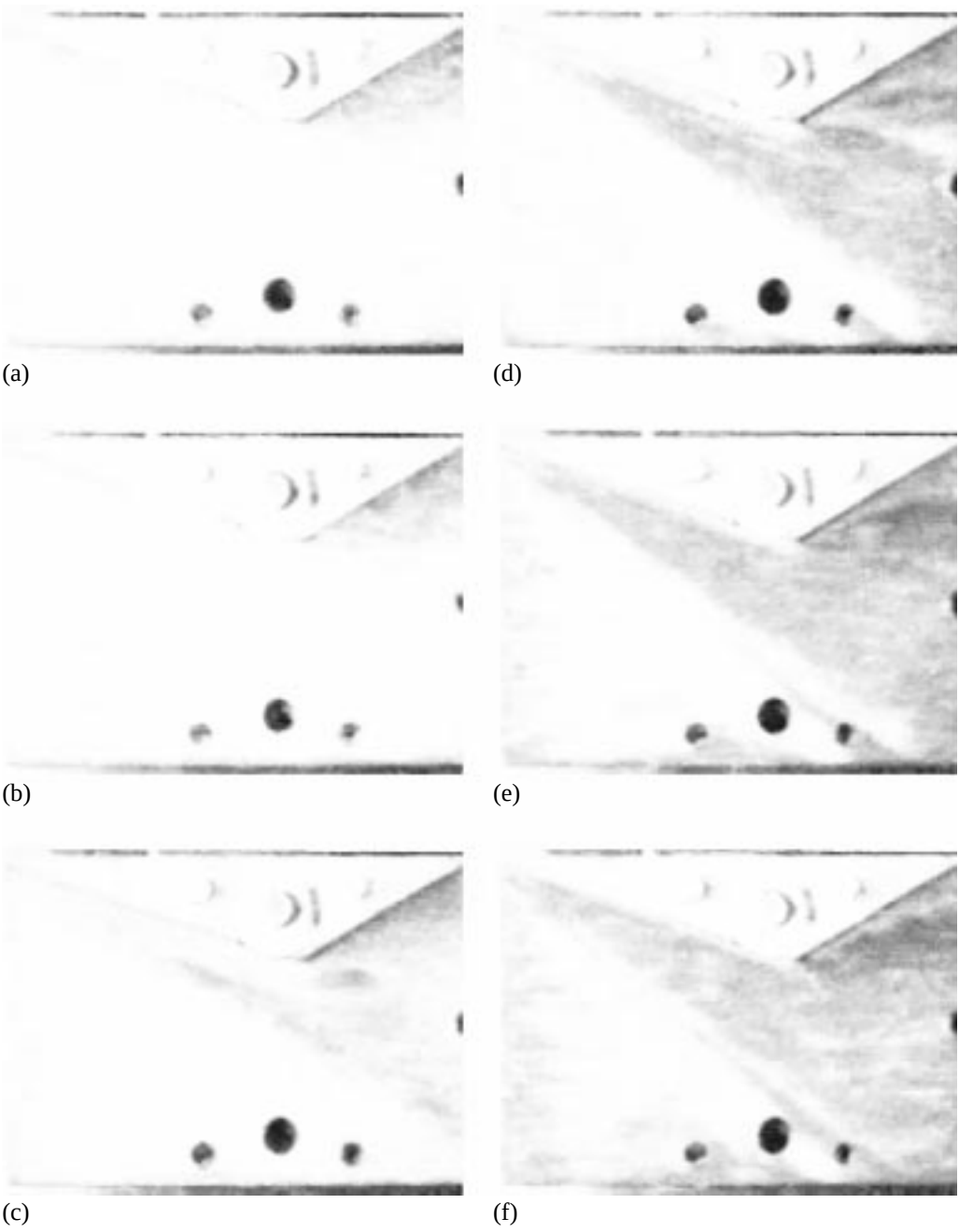

FIG. 8. Sequence of images showing colour play for test 42 (straight leading edge, single wedge). Flow is left to right. (a) −3.1, (b) 0.0, (c) 2.9, (d) 5.5, (e) 7.8 and (f) 9.5 s.

ery temperature) is below the lower temperature limit of the liquid crystal. Perspex was chosen for the model material because it is a good insulator. Even so, the surface temperature will not immediately attain the recovery temperature because of conduction of heat within the model. Modelling heat conduction within the substrate as one dimensional and being driven by the convective heat flux at the surface [28], the surface temperature can be used to infer the heat-transfer rate. The one-dimensional approximation will be valid as long as the thermal pulse from the test does not see the other side of the plate (or see the thermal pulse from the other side of the plate). For heat-transfer rates and test times typical of the UQ blowdown tunnel, a plate thickness of 15 mm should be sufficient to use the one-dimensional thermal modelling [10]. However, this will not be valid close to the leading edge of the endwall where the plate is not very thick. The large leading edge included angle (30^{o}) was chosen to increase the endwall thickness rapidly without producing a detached shock.

A sequence of images captured from the recorded video for run number 42 is shown in Fig. 8. The image in Fig. 8a shows the endwall plate prior to the test and a uniform surface temperature is indicated. The blue/green colour is consistent with the 24°C starting temperature and Table I. Associated with the hump in stagnation temperature at the start of the test (see Fig. 7), the liquid crystal layer flashes a bright blue colour as the flow arrives in the test section and the surface temperature rises momentarily. The peak of this temperature rise is captured in Fig. 8b and this is set as the zero reference time for the test. The TLC layer then goes back through hues of green, yellow and red as the temperature decreases and eventually becomes clear so that the black underlayer of paint is visible. In regions of higher heat transfer the endwall will go through these colour changes more rapidly than in regions of lower heat transfer. The image in Fig. 8c was captured when the first large region of the plate (upstream of the throat) turned black. This is the region where reattachment occurs and heat-transfer rates are the highest. The black region (Fig. 8d) has increased in size 2.6 s later and there is a line becoming black just upstream of the shock. This is clearer at the later times in the images in Figs 8e and f, suggesting that there may be more than one separation line and reattachment line in the interaction. Multiple separation and reattachment points associated with multiple horseshoe vortices have been observed in flows around obstructions in boundary layers [29], [30]. This shows the advantage of the high spatial resolution possible with TLC layers for identifying flow features that might otherwise be missed.

Test number 43 was conducted with the notched endwall and a single wedge (the geometry in Fig. 5b). This test has been chosen to compare with test 42 because the stagnation pressure and stagnation temperature time-histories are similar so that the rates at which the surface temperatures change for the two shots can be compared. The stagnation temperature time-histories for tests 42 and 43 are compared in Fig. 9. One difference was that the starting temperature for test 43 was approximately 1° C lower than that for test 42, but it can be seen that the subsequent time-histories of stagnation temperature are similar. Because of the lower starting temperature for test 43, for the same heat-transfer rates, the time taken for the TLC to reach its lower temperature limit and turn colourless will be marginally shorter than for test 42.

Figure 10 shows colour play images for test 43. The images were captured at the same times relative to the time of the stagnation-temperature peak as the images for test 42 in Fig. 8. The slightly lower initial starting temperature of the endwall plate for test 43 can be seen in the

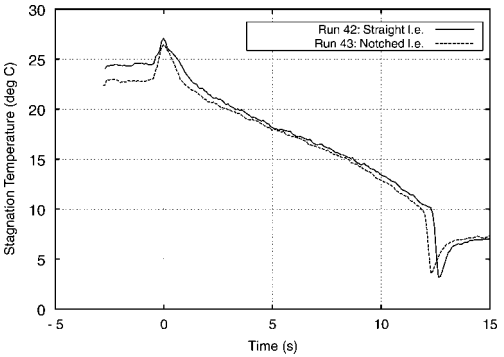

FIG. 9. Stagnation temperatures for test 42 (straight leading edge, single wedge) and 43 (notched leading edge, single wedge).

greener tinge of the image taken before flow start (Fig. 10a). The sequence of images shows similar trends to those discussed for test 42. Of interest here is the colour play in the region between the wedge and the notch of the inlet and a comparison of results in that region with those in the same region for the straight leading edge. The proportion of that area that shows black at time 2.9 s for the notched leading edge (Fig. 10c) appears slightly smaller than that for the same time for the straight leading edge (Fig. 8c). Taking into account the fact also that the endwall for test 43 started approximately 1°C less than that for test 42, this indicates a smaller heat-transfer rate in that region for the notched endwall. However, the differences in heat-transfer rates between the two tests in that region appear to be small based on these results and quantitative measurements are necessary to clarify the result. The results in that region at later times appear to be similar for the two inlet configurations.

5.2. *Double wedge cases*

The results for the endwall with the straight leading edge and two wedges (Fig. 5c) indicate a severe separation of the boundary layer on the endwall in the experiments. The heat-transfer rates to the endwall were significantly lower than for the single wedge results and even lower than the case with no wedges. The sequence of images captured for test number 47, with the double wedge, straight leading edge geometry, is shown in Fig. 11. It can be seen that there are large portions of the endwall that have still not reached the clearing temperature of the TLC mixture at the end of the test, indicating low heat-transfer rates.

The pressures measured in test 47 are shown in Fig. 12. The pressure measurement on the wedge indicates that the flow is not choked between the wedges. If it was choked the pressure there would be near to the static pressure behind a normal shock from Mach 3; this pressure level is indicated in Fig. 12 as “choked (theory)”. Note that the pressure measured on the wedge is well below this level but that it is also further above the level expected on the wedge than for the single wedge case and also for the notched leading edge case (see below). The higher pressure on the wedge is consistent with an increase in the effective displacement thickness of the boundary layer on the endwall that would occur with a significant separation.

Test 49 had the double wedge geometry with the notched endwall (Fig. 5d) and the separation observed for test 47 was not present in test 49. The sequence of images captured from the video tape for test 49 is shown in Fig. 13. As would be expected, the TLC in the region between

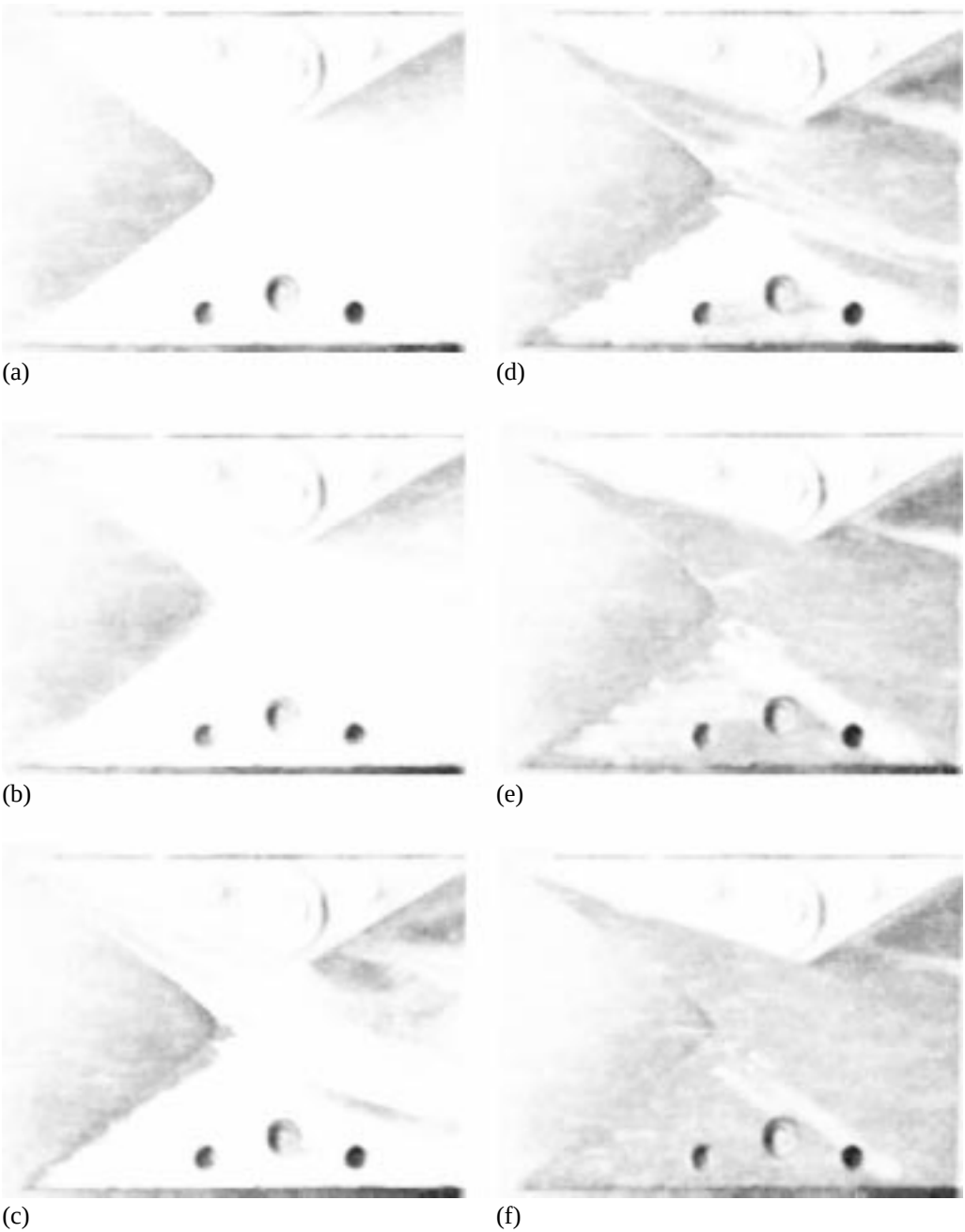

FIG. 10. Sequence of images showing colour play for test 43 (notched leading edge, single wedge). Flow is left to right. (a) −3.1, (b) 0.0, (c) 2.9, (d) 5.5, (e) 7.8 and (f) 9.5 s.

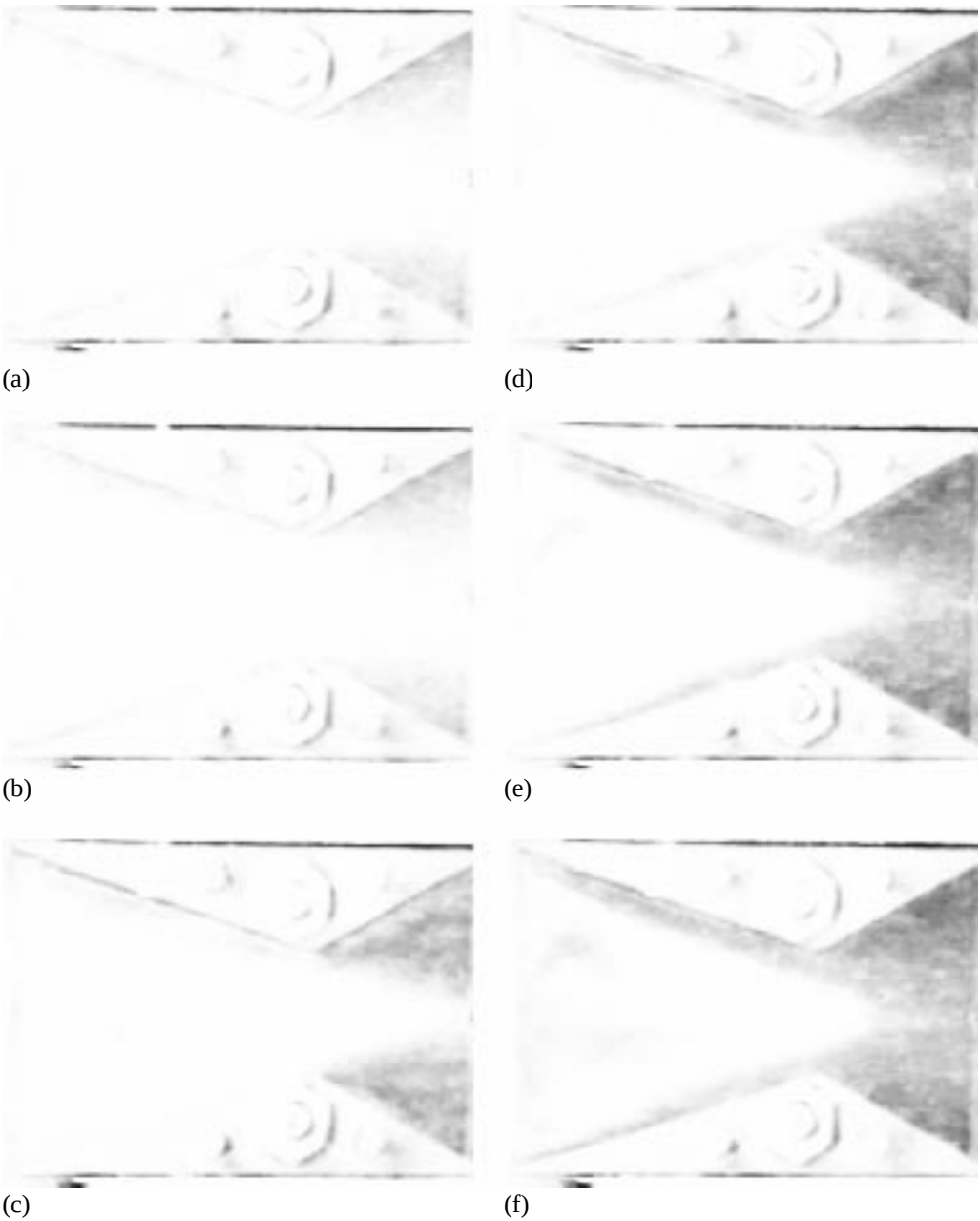

FIG. 11. Sequence of images showing colour play for test 47 (straight leading edge, double wedge). Flow is left to right. (a) −3.1, (b) 0.0, (c) 2.9, (d) 5.5, (e) 7.8 and (f) 9.5 s.

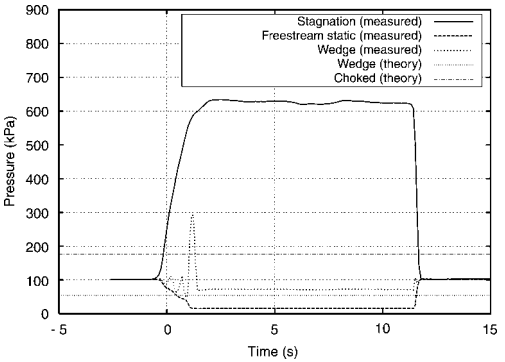

FIG. 12. Pressures for test 47 (straight leading edge, double wedge).

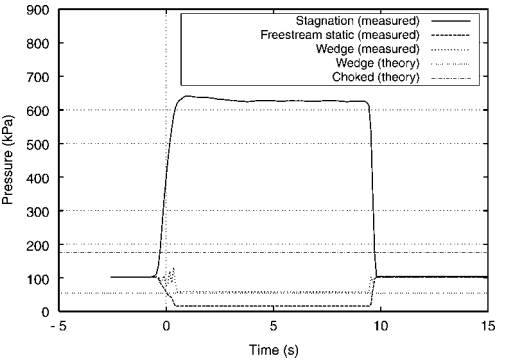

FIG. 14. Pressures for test 49 (notched leading edge, double wedge).

the wedge and the notch shows similar colour play to that observed for the single-wedge case for the notched leading edge (compare with Fig. 10). The colour play for the endwall near the second wedge is also similar. The much more rapid cooling of the endwall for test 49 compared with test 47 is attributed to the absence of a gross separation for the notched inlet.

The pressures measured for test 49 are shown in Fig. 14. It can be seen that the pressure on the wedge is close to the result for the single wedge and lower than for test 47. This again is taken as evidence of the absence of a large separated region for test 47.

6. Conclusion

Broadband thermochromic liquid crystals have been used to give qualitative measurements of the heat transfer to the simulated cowl of scramjet inlet configurations in a Mach 3 blowdown tunnel. The heat-transfer indication has been obtained without actively heating or cooling the test gas or test model. The driving temperature difference for heat transfer was the natural temperature difference that exists in a supersonic blowdown tunnel between the model temperature and the recovery temperature when the test gas in the reservoir and the test model start from ambient temperature. This is a simple technique that can easily be applied to test models for preliminary heat-transfer rate indications. It allows features to be observed with high spatial resolution. Subsequent quantitative measurements can then be made using other techniques. Note however that, with additional measurements, it should be possible to make quantitative measurements of heat transfer using the broadband TLC layer [10].

The comparison of the performance of a scramjet inlet with a notched cowl with that for a straight cowl indicates that the notched cowl can potentially avoid boundary layer separation. The results indicate that there may be a small advantage for the notched cowl in terms of reduced heat-transfer rates but quantitative measurements of heat transfer for the two inlet geometries are required to verify this.

Acknowledgements

This work was supported by the Australian Research Council.

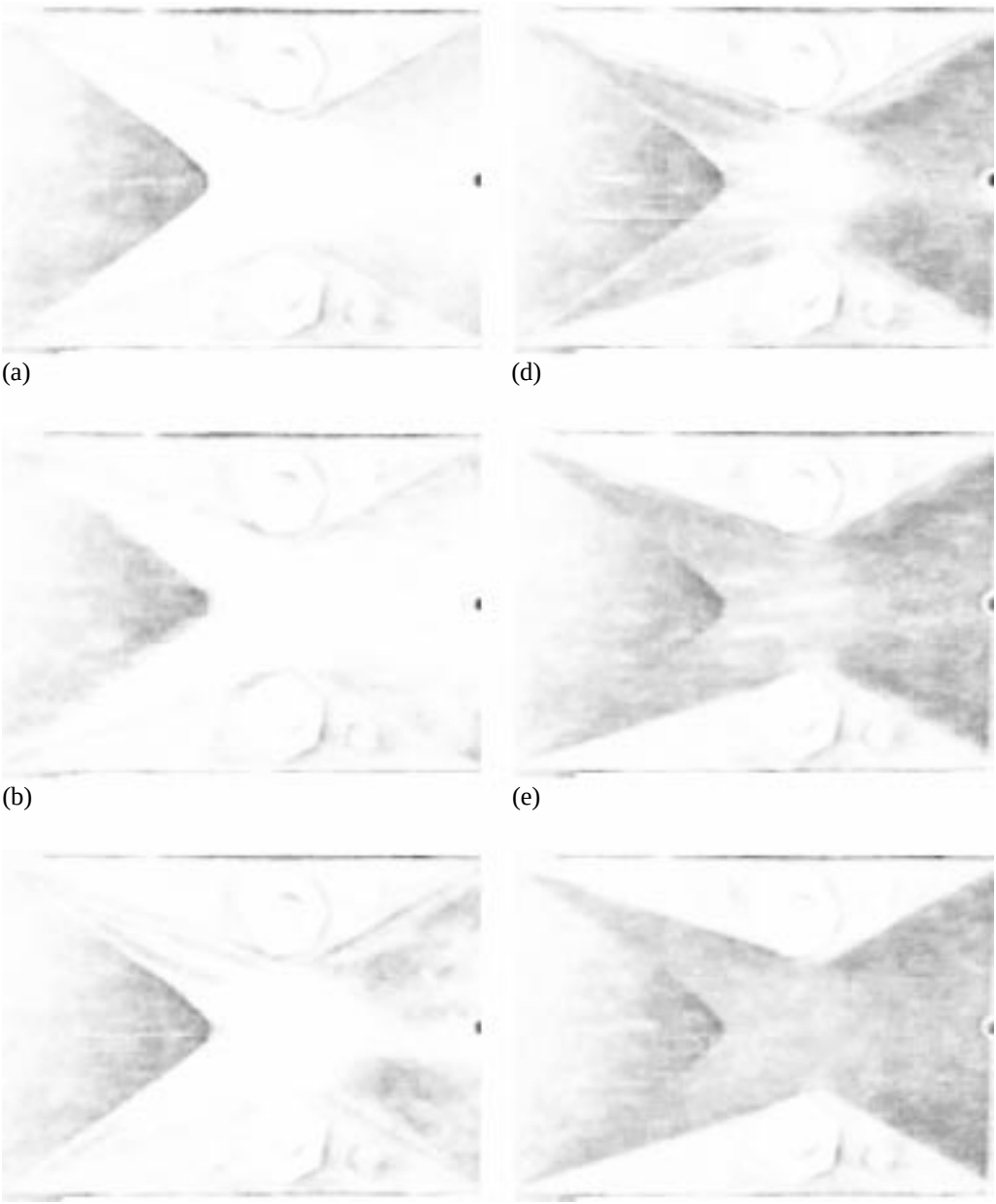

FIG. 13. Sequence of images showing colour play for test 49 (notched leading edge, double wedge). Flow is left to right. (a) −3.1, (b) 0.0, (c) 2.9, (d) 5.5, (e) 7.8 and (f) 9.5 s.

References

1. E. J. Klein, Application of liquid crystals to boundary-layer flow visualization, *AIAA Paper 68-0376* (1968).

2. Z. Wang, P. T. Ireland, S. T. Kohler and J. W. Chew, Heat transfer measurements to a gas turbine cooling passage with inclined ribs, *J. Turbomach.*, **120**, 63–69 (1998).

3. P. T. Ireland and T. V. Jones, Liquid crystal measurements of heat transfer and surface shear stress, *Measurement Sci. Technol.*, **11**, 969–986 (2000).

4. G. Engels, R. E. Peck and Y. Kim, Investigation of a quasi-steady liquid crystal technique for film cooling heat transfer measurements, *Expl Heat Transfer*, **14**, 181–198 (2001).

5. C. R. B. Day, M. L. G. Oldfield and G. D. Lock, The influence of film cooling on the efficiency of an annular nozzle guide vane cascade, *J. Turbomach.*, **121**, 145–151 (1999).

6. M. A. Zanchetta and R. Hillier, Boundary-layer transition on slender blunt cones at hypersonic speeds, *Proc. 20th Int. Symp. on Shock Waves* (H. H. B. Sturtevant and J. E. Shepherd, eds), World Scientific, pp. 699–704 (1996).

7. G. T. Roberts, P. H. Schuricht and N. R. Mudford, Heating enhancement caused by a transverse control jet in hypersonic flow, *Shock Waves*, **8**, 105–112 (1998).

8. Y. Lee, G. Settles and C. Horstman, Heat transfer measurements and computations of swept-shock-wave/boundary-layer interactions, *AIAA J.*, **32**, 726–734 (1994).

9. T. T. Evans and A. J. Smits, Measurements of the mean heat transfer in a shock wave-turbulent boundary layer interaction, *Expl Thermal Fluid Sci.*, **12**, 87–97 (1996).

10. D. J. Mee, H. S. Chiu and P. T. Ireland, Techniques for detailed heat transfer measurements in cold supersonic blowdown tunnels using thermochromic liquid crystals, *Int. J. Heat Mass Transfer*, **45**, 3287–3297 (2002).

11. M. K. Smart, Optimization of two-dimensional scramjet inlets, *J. Aircraft*, **36**, 430–433 (1999).

12. Y. P. Goonko and I. I. Mazhul, Some factors of hypersonic inlet/airplane interactions, *J. Aircraft*, **39**, 37–50 (2002).

13. S. D. Holland and J. N. Perkins, Inviscid parametric analysis of three-dimensional inlet performance, *J. Aircraft*, **31**, 610–615 (1994).

14. T. Shimura, N. Sakuranaka, T. Sunami and K. Tani, Thrust, lift and pitching moment of a scramjet engine, *J. Propulsion Power*, **17**, 617–621 (2001).

15. D. J. Mee, R. J. Stalker and J. L. Stollery, Glancing interactions between single and intersecting oblique shock waves and a turbulent boundary layer, *J. Fluid Mech.*, **170**, 411–433 (1986).

16. T. J. Garrison and G. S. Settles, Flowfield visualization of crossing shock-wave/boundary layer interactions, *AIAA Paper 92-0750* (1992).

17. D. V. Gaitonde, M. R. Visbal, J. S. Shang, A. A. Zheltovodov and A. I. Maksimov, Sidewall interaction in an asymmetric simulated scramjet inlet configuration, *J. Propulsion Power*, **17**, 579–584 (2001).

18. A. Kumar, D. J. Singh and C. A. Trexler, Numerical study of the effects of reverse sweep on scramjet inlet performance, *J. Propulsion Power*, **8**, 714–719 (1992).

19. J. J. Korte, D. J. Singh, A. Kumar and A. H. Auslander, Numerical study of the performance of swept curved compression surface scramjet inlets, *J. Propulsion Power*, **10**, 841–847 (1994).

20. F. S. Billig, Supersonic combustion ramjet missle, *J. Propulsion Power*, **11**, 1139–1146 (1995).

21. A. Paull, R. J. Stalker and D. J. Mee, Experiments on supersonic combustion ramjet propulsion in a shock tunnel, *J. Fluid Mech*., **296**, 159–183 (1995).

22. M. K. Smart, Design of three-dimensional hypersonic inlets with rectangular-to-elliptical shape transition, *J. Propulsion Power*, **15**, 408–416 (1999).

23. R. H. Korkegi, A simple correlation for incipient turbulent boundary-layer separation due to a skewed shock, *AIAA J.*, **11**, 1578–1579 (1973).

24. D. D. Knight, C. C. Horstmann, B. Shapey and S. Bogdonoff, Structure of supersonic turbulent flow past a sharp fin, *AIAA J.*, **25**, 10, 1331–1337 (1987).

25. G. S. Settles and F. K. Lu, Conical similarity of shock/boundary-layer interactions generated by swept and unswept fins, *AIAA J.*, **23**, 1021–1027 (1985).

26. R. D. Neumann and J. R. Hayes, The effects of test scale and facility details on the flow field features of supersonic three-dimensional fin/plate interactions, *AIAA Paper 2002–0976*, Jan. 2002.

27. G. Degrez and J. J. Ginoux, Surface phenomena in a three-dimensional skewed shock wave/laminar boundary-layer interaction, *AIAA J.*, **22**, 1764–1769 (1984).

28. D. L. Schultz and T. V. Jones, Heat transfer measurements in short duration hypersonic facilities, *AGARDograph 165*, (1973).

29. C. J. Baker, The laminar horseshoe vortex, *J. Fluid Mech.*, **95**, 347–367 (1979).

30. M. R. Visbal, Structure of laminar juncture flows, *AIAA J.*, **29**, 1273–1282 (1991).